ADVANCED ENERGY MATERIALS
www.advenergymat.de

Solvent Engineering for Scalable and Sustainable Fabrication of Lead-tin Perovskite Solar Cells

*Lijun Chen, Filippo Tavormina, Lorenzo Di Mario, Matteo Pitaro, Giuseppe Portale, Norberto Masciocchi, Antonietta Guagliardi, and Maria Antonietta Loi**

Hybrid lead-tin (Pb-Sn) perovskites have emerged as a promising avenue for photovoltaic technology with reduced toxicity and optimized bandgap. However, scaling up Pb-Sn perovskite solar cells (PSCs) from laboratory to industrial scale involves tackling challenges associated with scalable preparation technologies and the sustainability of solvents, the latter representing by far the major component of the reactant mixture(s). Here, innovative low-toxic solvent mixtures are proposed for a two-step blade-coating deposition process of the active perovskite layer: initially, diethylformamide (DEF) and dimethylsulfoxide (DMSO) (in 9:1 volume ratio), for processing the inorganic components of hybrid Pb-Sn perovskites (first step); then, in a second step, isopropanol (IPA) and 2-methyl-2-butanol (2M2B) (in 3:2 volume ratio) for the organic components, promoting the diffusion of the organic cation and the full precursor conversion to perovskite. Employing this low-toxic solvent engineering, low-D/3D Pb-Sn perovskites are successfully prepared with a champion power conversion efficiency (PCE) of 14.2%. Additionally, the devices prepared with both solvent systems retain more than 90% of their initial PCE after storage under an inert atmosphere for ≈2 months. This study represents a significant step toward understanding industrial viability, where not only efficiency but also sustainability of the production process should be considered.

1. Introduction

Metal halide PSCs are highly attractive devices, due to their high performance, solution processability, forecasted printability, and low-cost source materials used in the overall processing. Nowadays, the PCE of single-junction PSCs has reached a bottleneck stage, with a record efficiency of 26.7% for a small area of 0.052 cm^2, 24.74% for a larger area of 1.04 cm^2, and 22.6% for a minimodule of 20.25 cm^2,[1–3] approaching the Shockley–Queisser limit.[4,5] Further improvements in efficiency are expected from the development of tandem structures combining a narrow bandgap bottom cell with a wide(r) bandgap front cell.[6] While at the moment the most investigated tandem devices use silicon for the narrow band gap sub-cell, in perovskite-perovskite tandems, the narrow bandgap is achieved by alloying Pb- and Sn-based perovskites.[7,8] In recent years, significant progress has been made in optimizing the active layer crystalline quality,[9] charge carrier extraction,[10] and band alignment of narrow-bandgap Pb-Sn PSCs.[6–11] These advances allowed all-perovskite tandem solar cells to achieve a PCE of 28.5%.[12]

However, at this point of development of the field, it is becoming important to give due consideration also to the safety, environmental, and health issues associated with the processing of these materials, fostering the development of non-harmful large-scale production.[13] The broader topic of sustainability related with PSCs has already been identified as a subject of extensive interest in both the academic and industrial environments, therefore, an investigation that encompasses a wide range of

L. Chen, F. Tavormina, L. D. Mario, M. Pitaro, G. Portale, M. A. Loi
Zernike Institute for Advanced Materials
University of Groningen
Nijenborgh 4, Groningen 9747 AG, The Netherlands
E-mail: m.a.loi@rug.nl

The ORCID identification number(s) for the author(s) of this article can be found under https://doi.org/10.1002/aenm.202405941

DOI: 10.1002/aenm.202405941

L. Chen, M. A. Loi
CogniGron (Groningen Cognitive Systems and Materials Center)
University of Groningen
Nijenborgh 4, Groningen 9747 AG, The Netherlands
F. Tavormina, N. Masciocchi
Dipartimento di Scienza e Alta Tecnologia and To.Sca.Lab.
Università dell'Insubria
via Valleggio 11, Como I-22100, Italy
A. Guagliardi
Istituto di Cristallografia and To.Sca.Lab.
Consiglio Nazionale delle Ricerche
via Valleggio 11, Como 22100, Italy

device realization aspects, including solvents, deposition methods, and the longevity of the active material, could prove both insightful and timely. Given that the solvent constitutes the most abundant component (in weight and volume) of the solution deposition process, it is crucial to carefully screen and select different options.

To date, the preparation of efficient Pb-Sn PSCs involves hazardous and environmentally unfriendly solvents, such as dimethylformamide (DMF). DMF is included in the Candidate List of Substances of Very High Concern (SVHC) by the European Chemical Agency,[14] and in Class 2 (solvents of inherent toxicity) by the US Food and Drug Administration,[14] thus posing significant obstacles to the scalability of PSCs, during production, usage, clearance and ultimate disposal of solvents.

Searching for low-toxicity solvent alternatives, the usage of several non-noxious polar aprotic solvents has been reported for lead or tin perovskite systems, including γ-butyrolactone (GBL) and γ-valerolactone (GVL), among others.[15–18] Additionally, by processing the active layer using low toxicity ionic liquid (methylammonium acetate), the Pb-Sn perovskite devices reached a champion PCE of 15.96% when processed by spin coating in air.[19] DEF[20] is a less explored solvent in the perovskite field; while being not totally harmless, DEF is five times less toxic than DMF (as revealed by the lethal dose LD_{50} values, see Table S1, Supporting Information), and therefore can be used as a more friendly proxy for DMF.

Efficient Pb-Sn perovskite devices thus far reported are typically fabricated at the laboratory-scale using the spin coating method, a method that is far from being compatible with the manufacturing of large solar modules.[21,22] For large prototypes and industrial applications, scalable techniques, such as blade coating, are preferred. Herein, the solvents used play a crucial role in determining the film thickness, its morphology, and crystallization. Solvent(s) should be selected looking at the solubility and stability of the precursor materials, along with the possibility to control the crystallization by temperature and solvent evaporation rate during the coating process.[23,24]

Another significant challenge toward the industrial exploitation of perovskite devices is their environmental stability. The insertion of large organic cations (LOCs) represents a well-established methodology for partially stabilizing the perovskite phase. Such stabilization may be achieved in two ways: *i)* through the direct action of LOC halides as passivating agents,[25–27] inserted between perovskite grains and interacting with their boundaries and their defects, or *ii)* through the formation of new species, that are pseudo-perovskite phases, which are less prone to deterioration.[28,29] Both 2D/3D composites and quasi-2D phases have been used; in the quasi-2D case, the octahedra slabs are separated by layers of LOCs. The number of octahedra and the optoelectronic properties of quasi-2D perovskites, in the most fortunate cases, can be tuned by suitably choosing the concentration and the stereochemical properties of LOCs.[30,31] We additionally highlight that the crystallization process of low-dimensional phases is heavily influenced by the solubility of the large organic salt within the solvent used for all other precursors (in the so-called one-step deposition procedure) or by the ability of the LOC to react directly and selectively on the preformed film (in a two-steps deposition procedure).[30]

In our previous work, we demonstrated the preparation of quasi-2D Pb-Sn perovskite composites through a two-step blade coating process,[32] achieving PSCs with remarkable stability and efficiency. However, this process still relies on the use of toxic solvents such as DMF. Considering all these factors, even at the laboratory scale when developing material/solvent formulations and processing protocols suitable for large scale deposition, reducing the toxicity of the solvents employed is of the highest relevance.

Herein, we present a multifaceted approach addressing the crucial issues of efficiency, and sustainability of PSCs. Our low-D/3D Pb-Sn perovskite composites have been successfully fabricated with two-step blade coating based on two different solvent mixtures: DEF/DMSO and (IPA/2M2B). The introduction of DEF instead of DMF decreases enormously the toxicity of the process, whereas the IPA/2M2B mixture is here used instead of the most common IPA; indeed, this mixture shows a larger penetration depth than IPA alone, increasing the conversion of the precursor film deposited in the first step into the final perovskite, and, being slightly less polar, also limits the precipitation of LOC-based low-D materials in the earliest stages of crystallization. The champion device prepared by this method exhibits a record PCE of 14.2%. While this is a slight reduction in performance respect to devices prepared using the traditional solvent mixture (DMF/DMSO; PCE = 16.2%), it is also a demonstration that DMF can be fully removed from the process, increasing the potential for industrialization of perovskite devices. Interestingly, DEF/DMSO-prepared devices maintain ~90% of PCE when stored in the glovebox for about two months and after 110 h under continuous maximum power point (MPP) tracking without UV-filter.

2. Results and Discussion

2.1. Synthetic Aspects

Motivated by the necessity to address issues of scalable deposition methods and to mitigate the adverse effects of toxic solvents, low-D/3D Pb-Sn perovskite composites were fabricated using a two-step process[32,33] and a low-toxicity solvents blend. **Figure 1a** shows a schematic of the two-step blade coating process and the chemical structures of the different solvents employed.

The first step consists of depositing an inorganic precursor solution onto a hole transport layer (HTL), by blade-coating at controlled temperature, immediately followed by annealing to form a $(Pb_{0.5}Sn_{0.5})I_2$ film. The second step involves the deposition of an alcoholic solution of organic salt (FAI, MAI, and PEAI, PEA = phenylethylammonium) on top of the $(Pb_{0.5}Sn_{0.5})I_2$ film, ultimately resulting in the formation of an active layer of nominal composition $MA_{0.3}FA_{0.7}(Pb_{0.5}Sn_{0.5})(Cl_{0.04}I_{0.96})_3$. The first step was performed dissolving the precursors in two different solvent mixtures: DEF/DMSO and the more conventional DMF/DMSO. The solvent blend employed in the second step was a combination of 2M2B/IPA for the purpose of optimizing the conversion process respect to the pure IPA, which we reported earlier.[32] **Table 1** contains the detailed comparison of physical-chemical parameters of the used solvents; according to the CHEM21 selection guide of classical and less classical solvents,[34] DMF is

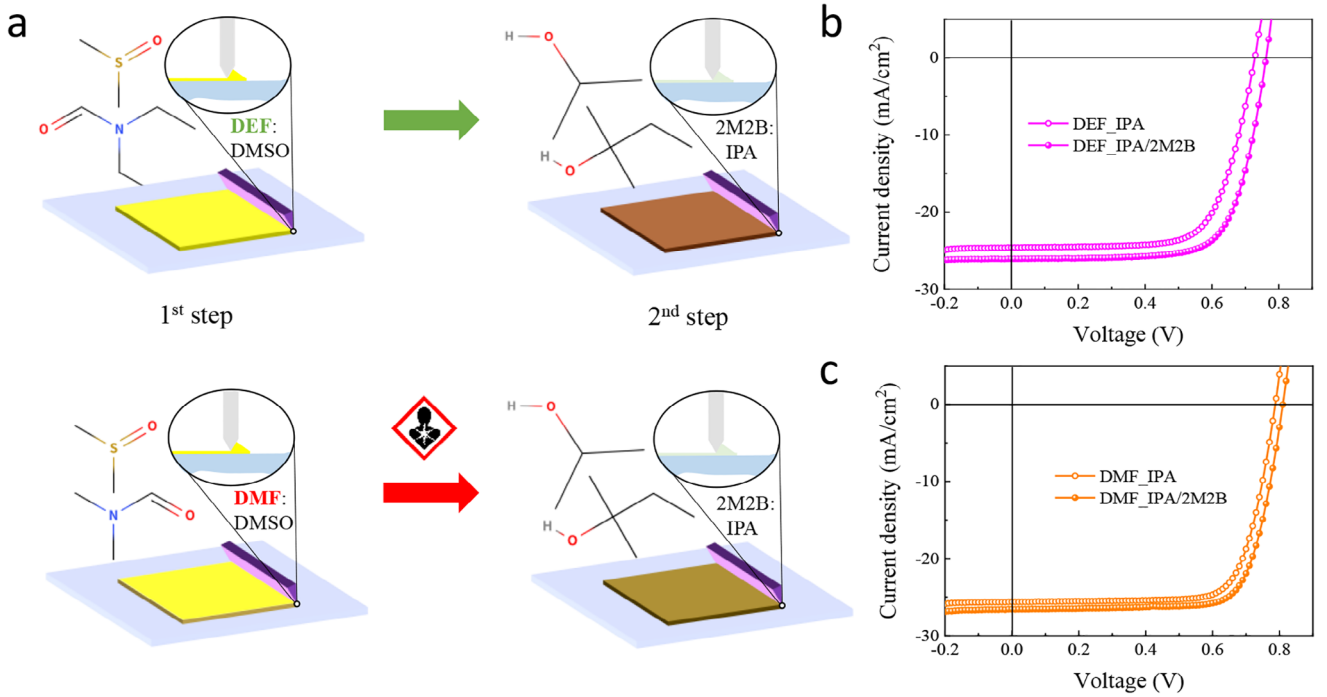

Figure 1. a) Schematic illustration of the two-step blade coating and the molecular structure of the solvents used in this work. b) J-V curves of the best Pb-Sn devices fabricated using the less-toxic solvent mixture for the first step, combined with IPA or IPA/2M2B for the second step. c) J-V curves of the best devices fabricated using the DMF-based solvent mixture for the first step, followed by IPA or IPA/2M2B treatment.

classified as being highly hazardous while DEF and the other solvents are listed as recommended reagents. In addition, it is important to underline that our scalable deposition strategy uses less than one-tenth of the solvents and precursors required by spin coating.

The challenge associated with the development of scalable solution-process deposition techniques for perovskites lies in the increased drying time and the elevated solvent content of the resulting films, making them susceptible to the coffee ring effect,[36] as well as the Marangoni effect,[37] and heterogeneous growth dynamics.[38] DEF, with a boiling point (177 °C) is comparable to DMF and DMSO, and can give rise to homogeneous films when the drying dynamics are optimized. In fact, although the Lewis basicity of DEF (expressed by the conventional Donor Number) is higher than that of DMF,[16] the lower dielectric constant of DEF results in a slightly weaker coordination ability against Pb^{2+}/Sn^{2+} cations,[20] thus leading to the formation of homogeneous films with low roughness; similar to findings reported for a single step spin-coating process.[20]

The chemical interactions between the two solvents sets and the perovskite precursors are investigated using FTIR and XRD. As illustrated in Figures S1 and S2 (Supporting Information), and summarized in Table S2 (Supporting Information), different adducts are obtained when using the DEF and DMF based solvent mixtures, without annealing. Briefly, the formation of DEF-containing complexes (in solution) may occur (Figure S2, Supporting Information), however, the weakly coordinating nature of DEF may be taken as responsible for the rarity of crystalline adducts with DEF in the annealed films (Figure S3, Supporting Information). For more details and a short discussion, please refer to the Supporting Information. Our finding is consistent with a Cambridge Structural Database search revealing the full absence of DEF-containing Pb or Sn species, while more than 150 adducts (each) of DMF or DMSO were found (only in part explained by their ubiquitous use).

Indeed, DEF is highly compatible with the initial step of blade coating deposition, wherein annealing temperatures are maintained at a relatively low level to minimize the occurrence, in the $(Pb_{0.5}Sn_{0.5})I_2$ film, of Sn-based defects. Thereafter, to facilitate the formation of the perovskite in the second stage of the process, it is essential to ensure the appropriate diffusion of the alcoholic solution, which allows a greater volume of $(Pb_{0.5}Sn_{0.5})I_2$ to be available for the reaction with the organic salts, thereby enhancing its conversion rate.[33,39] In this context, the co-solvent 2M2B, which has a higher boiling point, increased steric

Table 1. Summary of solvent parameters.

Solvent	Hazard[a)]	Scores[b)]	bp[c)]	D.N.[d)]	ϵ_r[e)]	Ranking
DMF	H360	3, 9, 5	153	26.6	38.2	Hazardous
DEF	H335	1, 2, 5	177	30.9	29.0	Recommended
DMSO	none	1, 1, 5	189	29.8	47.2	Recommended
IPA	H336	4, 3, 3	82	21.1	19.9	Recommended
2M2B	H336	3,4, 3	102	44.0[5]	5.8	Recommended

[a)] worst hazard code (from https://echa.europa.eu/it/regulations/reach/understanding-reach); [b)] safety, health, and environmental scores, values taken from;[34] [c)] normal boiling points in °C, values taken from;[35] [d)] donor number in *kcal mol*$^{-1}$, values taken from;[16] [e)] relative electric permittivity, *ibid*.

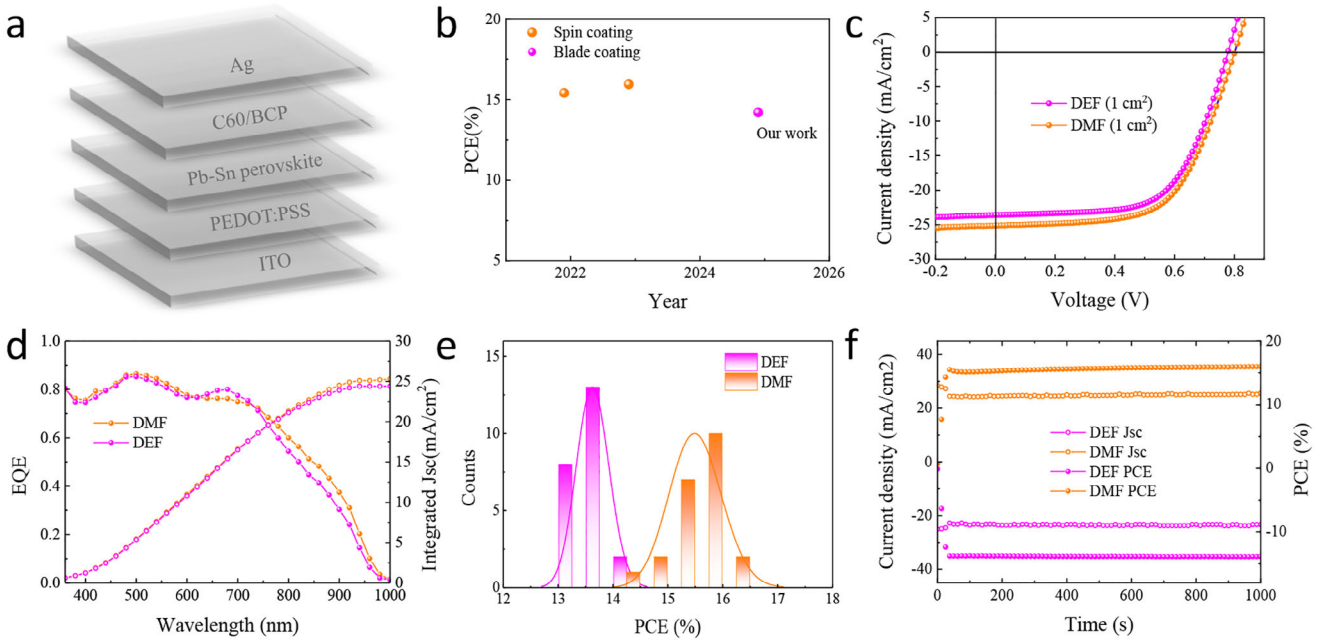

Figure 2. a) Schematic device structure of the fabricated perovskite solar cell. b) Reported efficiency of Pb-Sn PSCs prepared with low-toxicity solvents. c) J-V curves of the champion devices fabricated using DMF- or DEF-based mixtures with an active area of 1 cm^2. d) EQE spectra and integrated photocurrent of the devices. e) Statistical distribution of PCEs based on an active area of 0.04 cm^2 for the two different solvent systems. f) Steady-state power output of the devices (we used a *negative* scale to graphically distinguish the DMF/DEF traces).

hindrance, and decreased polarity respect to IPA, is useful in modulating the crystallization kinetics and can induce a greater degree of conversion.[40]

2.2. Device Performances

Figure 1 (in panels b and c) shows the current density-voltage (J-V) characteristics of devices fabricated using the DEF- and DMF-based solvent mixtures, respectively. A p-i-n architecture, which is composed by the ITO/PEDOT: PSS/Pb-Sn perovskite/C60/BCP/Ag (**Figure 2a**), is utilized. We found that by employing the IPA/2M2B solvent mixture for the organic salt solution in the second deposition step, markedly enhanced device performances are obtained (Tables S3 and S4, Supporting Information), for both devices prepared with DEF- and DMF-based mixtures (14.2% and 16.2% PCE, respectively). By contrast, the devices realized with pure IPA in the second step exhibited a slightly reduced efficiency, with values not exceeding 12.5% (DEF-mixture) and 15.1% (DMF-mixture) PCE. X-ray powder diffraction (XRD) measurements show that a tiny peak of the PbI_2/SnI_2 solid solution[41] is still present in the films after conversion utilizing IPA as solvent (Figure S3, Supporting Information). When a fraction of the IPA is replaced by 2M2B, the amount of unreacted PbI_2/SnI_2 vanishes. This indicates that 2M2B, with its higher boiling point (Table 1), facilitates the organic salts solution diffusion into the preformed $(Pb_{0.5}Sn_{0.5})I_2$ scaffold, thereby improving the conversion to the perovskite phase and consequently device performance. The presence of an unconverted phase in the final film results in a reduction in overall performances (PbI_2 and SnI_2 being electrical insulators) and may also accelerate the perovskite degradation. Therefore, all devices discussed in the following have been prepared by using IPA/2M2B mixtures in the second step.

As shown in Figure S4 and in Tables S4 (Supporting Information), a champion PCE of 14.2%, with V_{OC} (0.762 V), J_{SC} (26.09 $mA\ cm^{-2}$), and *FF* (72%) is obtained with the low-toxicity solvent mixtures, which, to the best of our knowledge, is one of the highest PCE for Pb-Sn PSCs prepared in scalable and environmentally friendly way (see Figure 2b).[19,42–45] For comparison, the highest PCE of the device prepared using the conventional, toxic DMF/DMSO mixture was 16.2% ($V_{OC} = 0.810\ V$, $J_{SC} = 26.59\ mA\ cm^{-2}$, and $FF = 75\%$; see Figure S4 and Table S6, Supporting Information). Importantly, devices with larger active areas demonstrated excellent scalability (see Figure 2c; Table S7, Supporting Information). DEF- and DMF-based devices with an area of 1 cm^2 showed PCE values of 11.5% and 12.3%, respectively. Therefore, the proposed combination of non-harmful solvents is a viable option for the scalable fabrication of Pb-Sn perovskite devices. The slightly lower efficiency of devices made with the less harmful solvents is compensated by the lower environmental impact of the device fabrication and, in an industrial perspective, by the lower cost involved in the disposal of the solvents. A reasonable explanation of the lower performance is later discussed, based on GIWAXS analysis.

The external quantum efficiency (EQE) spectra are shown in Figure 2d. The integrated J_{SC} values from the EQE spectrum are nearly equivalent: 24.4 and 25.3 mA cm^{-2} for DEF- and DMF-processed devices, respectively. The slightly lower values compared to the measured J_{sc} can be attributed to the significantly weaker light intensity used in our EQE measurements compared to standard AM1.5G conditions. The UV–vis absorption

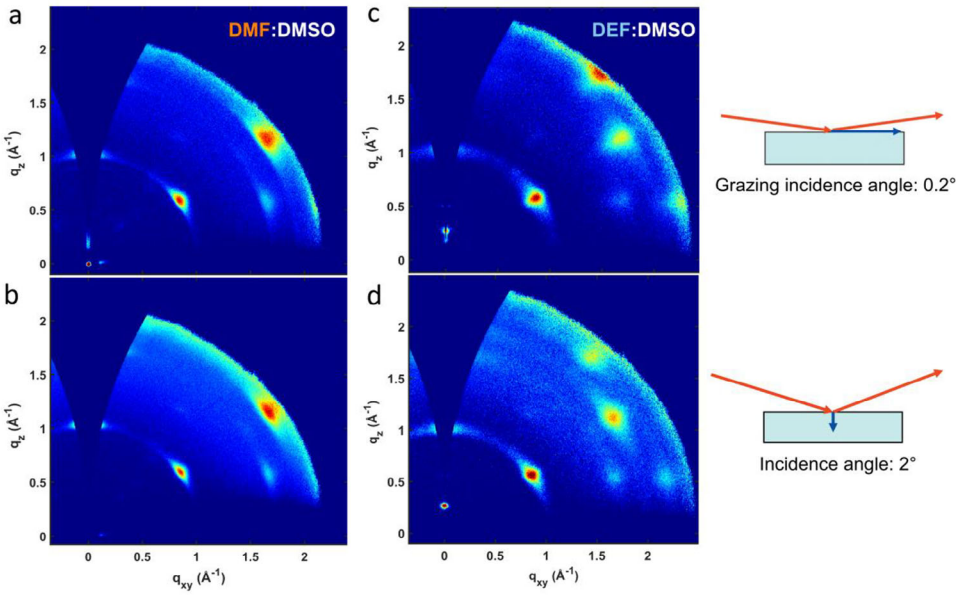

Figure 3. GIWAXS patterns of the perovskite films processed with DMF (left) and DEF (right), recorded using an incident angle of 0.2° (a,c) and 2.0° (b,d). Maximum measured $|\vec{Q}|$-values differ due to slightly different instrumental conditions. Indexed spots are portrayed in Figure S9 (Supporting Information). Here, $\vec{Q}$ is the scattering vector, $|\vec{Q}| = Q = 4\pi sin\theta/\lambda$ and q_{xy} and q_z are its components in the equatorial plane and axial direction, respectively. In the right panels, schematics of the grazing incidence geometry with angles exaggerated to visually appreciate their difference.

spectra reveal that both Pb-Sn perovskite films possess a similar absorption edge (1.27*eV*) (see Figure S5, Supporting Information), which is close to the value reported for similar composition.[46,47] A bandgap of 1.32 *eV* is derived from the inflection point of the measured EQE spectra for both films, which is slightly higher than the value obtained from UV–vis absorption. Figure 2e and Figure S6 (Supporting Information) demonstrate the reproducibility of photovoltaic parameters, with average PCE values from 20 devices prepared using DEF and DMF of 13.6±0.3% and 15.5%±0.5%, respectively. The average values of the V_{oc}, J_{sc}, and *FF* parameters are 0.75±0.01 *V*, 71.91%±1.31%, and 25.56±0.79 $mA\ cm^{-2}$ for DEF-, and 0.79±0.01 *V*, 26.36±0.55 $mA\ cm^{-2}$, and 74.82±0.66% for DMF-processed film. We further investigated the steady-state power output (shown in Figure 2f). The stabilized PCE of DEF-processed devices is 13.90% with an output current density of 23.56 $mA\ cm^{-2}$ at 0.59 *V* after continuous illumination for 1000 s. This PCE value is slightly lower than that of the DMF-processed device, which reached a stabilized PCE of 16.0% at 0.63 *V*.

2.3. Structural and Morphological Characterization

To gain a deeper insight into the influence of the solvent on the morphology of blade-coated films, scanning electron microscopy (SEM) and atomic force microscopy (AFM) measurements were performed (images are shown in Figures S7 and S8, Supporting Information). Therein, film grains look almost similar. Grain sizes, of ca. 100 *nm*, which are slightly larger for the DEF-processed films (see the magnified images in Panels b and d of Figure S7, Supporting Information), in line with the slightly higher boiling point of DEF, likely limiting supersaturation and generating less nucleation sites and thus retarding crystal growth. In the microscopic images, many triangular facets appear, which are interpreted as predominant (though uncommon) [111]-directed morphology (such as octahedra and cuboctahedra[50]), well in line with the preferred alignment of the crystallites detected in the GIWAXS experiments discussed later. AFM images (Figure S8, Supporting Information) reveal a comparable root-mean-square (RMS) surface roughness for both films (ca. 9 *nm*), showing that DEF enables the preparation of high-quality perovskite films, very much like those prepared by using DMF/DMSO in the first deposition step.[32]

GIWAXS measurements were performed to differentiate the structural/textural effects induced by the usage of different solvents. To ensure the closest possible sample quality to the one used in the real solar cell device, the perovskite films were deposited directly on a PEDOT:PSS layer, rather than on the ITO substrate, given that the crystal growth mechanism and, particularly, the final orientation of the perovskite film are susceptible to alteration by the characteristics of different surfaces.[48] **Figure 3** displays GIWAXS images obtained from perovskite films prepared with DMF and DEF at two distinct grazing incidence angles (0.2° and 2.0°, that is below and above the estimated critical angle of 0.27°[49]), ideally separating scattering from the close-to-surface and bulk regions within the films.

GIWAXS images of the DMF-processed films, in Figure 3a,b, show the occurrence of highly textured samples, both characterized by two different crystal orientation: (predominantly) along the [111] direction (as reported for the 3D α-$FAPbI_3$ phase[50] and low-D perovskites phases[51,52]) and, to a minor extent, along [100] (details are provided in Figure S9, Supporting Information). Though we have no mechanistic details of how the 3D perovskite forms from the metal diiodide film in the second blade-coating

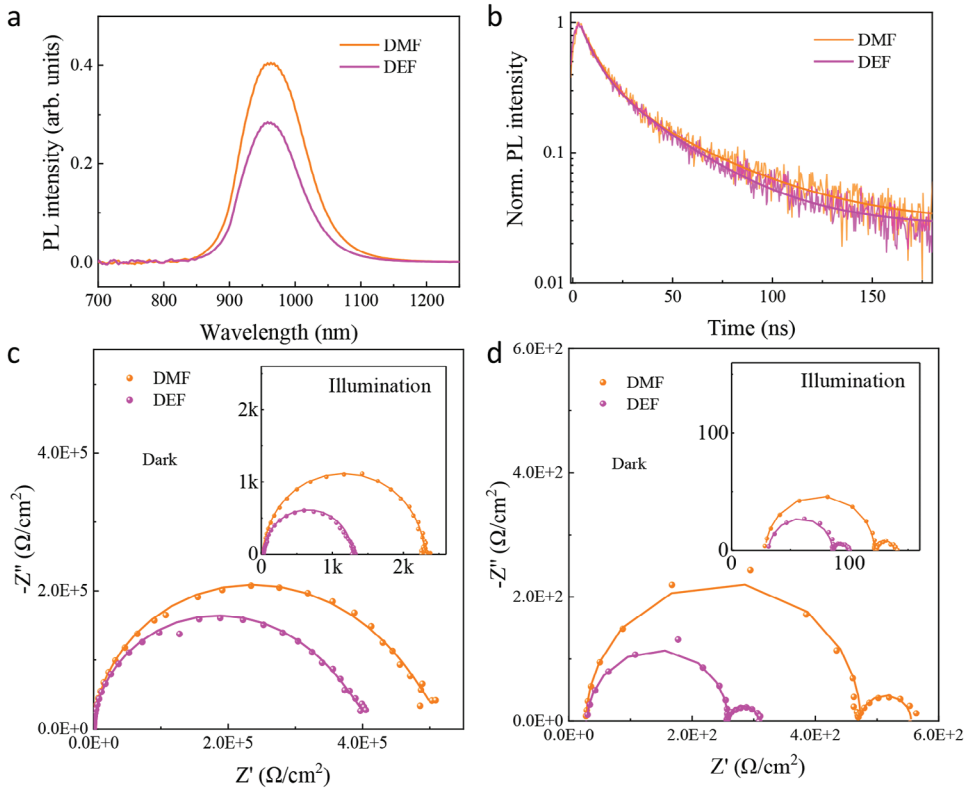

Figure 4. Photoluminescence measurements for perovskite films fabricated with DEF and DMF: a) steady-state photoluminescence; b) time-resolved photoluminescence. c) Nyquist plots of the devices under dark condition at short-circuit. Insert: under illumination. d) Nyquist plots of devices fabricated with different solvents under dark condition at open circuit. Insert: under illumination.

step, we note that in a very recent paper Liu et al.[53] demonstrated that, for spin coated and thermal annealed films of LOC doped perovskites, the [111] orientation results from the way low-*n* perovskites tend to grow, to larger *n* values, possibly through the intermediacy of MACl additive. Notwithstanding the presence of very low-Q streaks observable in Figure 3a (attributed to the substrate and to the perovskite surface roughness), no obvious low-D phases are detected on the surface nor deeper in the film (Figure 3b). In Figure 3c,d, the films processed from DEF display the same texture observed in panels a-b. More relevant is the presence of two spots at 0.263 and 0.491 $Å^{-1}$ in the low-q_z zone (as per Figure S10, Supporting Information), attributed to oriented crystal phase(s) with a longer periodicity than a 3D perovskite. The *d*-spacing associated with the 0.263 $Å^{-1}$ peak is approximately $d = \frac{2\pi}{Q}$ =23.9 Å, which we found consistent only with the *d*-spacing given by a 002 reflection of a low-D phase, characterized by a cell axis of 47.78 Å in length (ideally, $PEA_2(MA_{0.3}FA_{0.7})_{n-1}(Pb_{0.5}Sn_{0.5})_n(Cl_{0.04}I_{0.96})_{3n+1}$, with $n = 6$; see Figure S10, Supporting Information for the explanation of this estimate). Given the spot intensity observed in the diffraction data, it can be posited that the low-D phase at n = 6 is relatively modest in abundance. Moreover, it cannot be excluded that the perovskite film comprises a mixture of periodic and non-periodic phases in minor quantities (or with very small crystallites) that are not discernible with GIWAXS analysis. Finally, a very tiny signal, located at 0.491 $Å^{-1}$ and shown in Figure S10 (Supporting Information) could not be properly assigned. Therefore, highly oriented and crystalline films were achieved using low-toxic solvents, demonstrating the feasibility of our scalable and sustainable approach for fabricating Pb-Sn devices. Based on the above observations, the minor difference observed in solar cells performances may be (partially) attributed to the (measurable) occurrence of low dimensional phases in this sample, with respect to the DMF-based one, which may be responsible for the less effective current transport (lower *Jsc*).

2.4. Spectroscopic and Functional Characterization and Device Stability

To gain more insight into the mechanism behind device performance variations determined by the solvents utilized in the first step, we conducted steady-state photoluminescence (PL) and time-resolved PL (TRPL) measurements to elucidate the charge carrier dynamics and trap states density (see **Figure** 4a,b). The PL peaks of both films are located at 960 nm, but the film processed with DEF exhibits a slightly weaker PL intensity, which indicates enhanced nonradiative losses in the DEF processed sample. The TRPL curves were fitted using a bi-exponential decay model, and the resulting parameters are summarized in Table S8 (Supporting Information). The DMF-processed film exhibited a slightly longer PL lifetime (33.85 *ns*) compared to the DEF film (30.27 *ns*), again showing a slightly larger non radiative component for

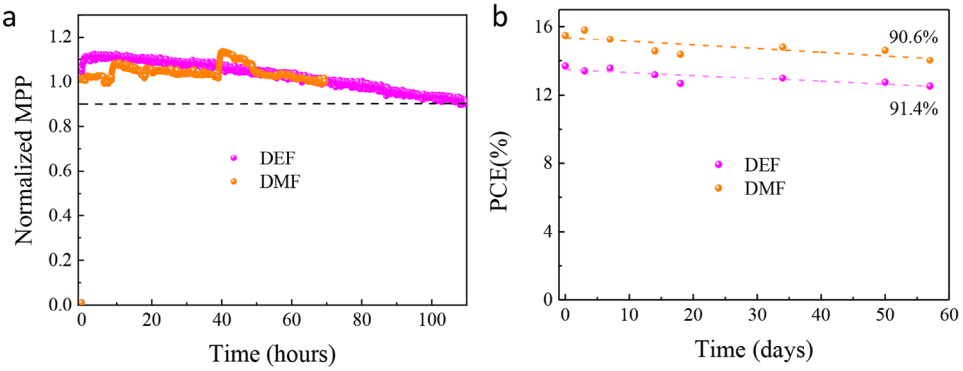

Figure 5. Stability of non-encapsulated solar cells fabricated with DEF and DMF solvents: a) Operation stability measured at MPP under continuous illumination (AM 1.5 G) (the DMF-processed samples show some fluctuations due to changes of the environment in the glove box during the measurement period); b) Shelf-life stability measured under N_2 atmosphere.

the DEF-processed films. In addition, the dark J-V curves of the two devices show similar diode behavior and leakage current density (see Figure S11, Supporting Information), again confirming their similar (electrical) film quality and recombination behavior.

The charge recombination process was further analyzed using electrochemical impedance spectroscopy (EIS), with the raw data and model fitting results presented in Figure 4c,d. We compared the Nyquist plots under illumination (AM 1.5 G) and in the dark, at both open-circuit and short-circuit conditions. As shown in Figure 4 and detailed in Tables S9 and S10 (Supporting Information), the impedance spectra were fitted using different equivalent circuit models. The high-frequency components are associated with charge transfer and interfacial recombination at the perovskite/transport layer interfaces, while the low-frequency components correspond to bulk charge carrier recombination and ion migration within the perovskite layer.[54] Under short-circuit conditions, illumination reduces the semicircle diameter in the Nyquist plots, indicating lower transport resistance and improved charge accumulation and extraction. Among the samples, the DMF-processed device exhibits slightly better charge transfer and extraction characteristics. At open-circuit conditions, an additional arc appears, attributed to ion migration. The DMF-based sample shows a larger recombination resistance, suggesting reduced charge recombination within the perovskite layer, which is consistent with our previous analysis. All extracted parameter values are summarized in Tables S9 and S10 (Supporting Information). Notably, both curves shown in Figure 4 for the DMF- and DEF-processed devices are similar and can be fitted with the same equivalent circuit model, providing further evidence that both solvents result in comparable film quality when using blade coating.

Finally, we also investigated the long-term stability of the prepared solar cells. We first tracked the operational stability of the devices in an inert atmosphere. The devices (without encapsulation) were measured at the MPP under one sun illumination (AM 1.5 G) without any UV-filter. As illustrated in **Figure 5**a, the DEF solvent-processed device retains ≈90% of its initial PCE after 110 h, while the DMF-processed device shows no significant degradation after 70 h, indicating very similar stability behavior for the two solvents. Fluctuations in MPP are likely due to defect healing induced by serendipitous oxygen exposure.[55] A phenomenological data analysis, which aims at recovering kinetic aspects of these fluctuations, is proposed in Figure S12 (Supporting Information).

Thermal stability is also reported in the supporting information. In addition, the shelf lifetime was evaluated under dark conditions in an N_2-purged glovebox, as shown in Figure 5b. Both devices-maintained ca. 91% of their initial PCE, the very small difference (if any at all) being possibly attributed to the presence of minor amounts of low-D crystalline phase, known to stabilize the active layer over time. In summary, we successfully fabricated Pb-Sn devices using low-toxicity solvents and scalable processing techniques. We believe these devices display slightly lower PCE because of the increased portion of low dimensional phases detected by the GIWAXS investigation. Low dimensional phases are indeed well known to hinder charge transport and can be at the origin of the lower current displayed by the devices utilizing DEF in the first step. The second step, carried out with different solvent blends (pure IPA and IPA:2M2B), led to variations in performance, which can be attributed to two distinct phenomena yielding the same final effect. The higher boiling point of 2M2B prolongs the reaction time between the precursors during the second step, enhancing the conversion of $Pb_{0.5}Sn_{0.5}I_2$ to the perovskite phase.

3. Conclusion

In this work, efficient low-D/3D Pb-Sn PSCs have been successfully prepared through the fabrication with scalable two-step deposition methods based on the low-toxicity DEF solvent substituting the noxious DMF one in the first deposition step. Additionally, we found that a new combination of protic solvents, and the IPA/2M2B mixture, in the second stage favors the full conversion of the PbI_2/SnI_2 film into the sought perovskite. These perovskite films display high uniformity, high crystallinity, low trap states, and efficient charge carrier transport characteristics. The blade-coating deposition process enabled the attainment of a high PCE, 14.2%, using (mixtures of) low-toxic solvents, thereby demonstrating the effectiveness of this low-toxic deposition approach. Additionally, the prepared devices maintain over 90% of the initial PCE upon storage in inert conditions and in the dark

for ≈2 months, or even after continuous MPP tracking under illumination for 110 h. While the devices fabricated with DMF show 2% higher efficiency, we believe that in the long run efficiency shall not be the only relevant parameter determining the foreseeable success of a technology, but other factors as the variability of the materials involved, the environmental impact of the device fabrication and its scalability will play a major role.

4. Experimental Section

Materials: poly(3,4-ethylenedioxythiophene) polystyrene sulfonate (PEDOT: PSS (AI 4083)) was purchased form Heraeus. Formamidinium iodide (FAI, >98%), methylammonium iodide (MAI, >98%), phenethylammonium iodide (PEAI, >98%), methylamine chloride (MACl, >98%), bathocuproine (BCP, >99%), N, N-Diethylformamide (DEF, >99.0%) were purchased from TCI EUROPE N. V. Dimethyl sulfoxide (DMSO, 99.8%) and N, N-dimethylformamide (DMF, 99.8%) were acquired from Alfa Aesar. Tin (II) iodide (SnI_2, 99.99%), Lead (II) iodide (PbI_2, 99.99%), Tin (II) Fluoride (SnF_2, 99%), fullerene (C_{60}, 99.9%), isopropyl alcohol (IPA, 99.7%), and 2-methyl-2-butanol (2M2B, 99%) were obtained from Sigma-Aldrich.

Perovskite Film Deposition: The inorganic precursor solution was prepared by mixing 0.125 mmol of PbI_2, 0.125 mmol of SnI_2, and 0.0125 mmol of SnF_2 in 0.5 mL DEF/DMSO (DEF: DMSO = 9:1) for low-toxic system or 0.5 *mL* DMF/DMSO (DMF: DMSO = 9:1) for the reference system. The organic salts precursor solution was prepared by mixing 0.16 mmol of FAI, 0.04 mmol of MAI, 0.025 mmol of PEAI, and 0.03 mmol of MACl in 0.5 *mL* of IPA/2M2B (IPA:2M2B = 3:2). All solutions were stirred overnight at room temperature and then filtered with 0.22 µm PTFE filter before use. The inorganic film of $(Pb_{0.5}Sn_{0.5})I_2$ formulation was first deposited by blade coating in N_2-filled glovebox ($O_2 < 0.1$, $H_2O < 0.1$ ppm). The blade coating height, temperature, and speed were set to 900 µm, 50 °C, and 20 mm s^{-1}, respectively. The films were immediately annealed at 50 °C for 10 min. After cooling, the organic solution was deposited on the inorganic film at 50 °C by a second blade coating process with same parameters as the first step, and followed by thermal annealing at 100 °C for 10 min.

Device Fabrication: Patterned ITO substrates (30 × 30 mm^2) as bottom electrodes were first cleaned and dried for use. Before depositing the PEDOT:PSS layer, ITO glasses were treated in a UV-O_3 chamber for 30 min. The HTL of PEDOT:PSS was fabricated by spin coating (at 3000 rpm for 60 *s*) and subsequent annealing (at 140 °C for 20 min) in air. At this stage, the substrates were transferred into the glovebox to deposit the perovskite films. The active layer of Pb-Sn perovskite films was fabricated with a two-step blade coating as previously described. After that, the electron transport layers of C_{60} (30 nm)/BCP (6 nm) were thermally evaporated under a vacuum of 10^{-7} mbar. Finally, the top electrode of Ag (100 nm) was deposited to form a completed device.

Characterization: The J-V curves of the perovskite solar cells were measured using a Keithley 2400 source meter under AM 1.5 G solar illumination in N_2-filled gloveboxes, with a scan rate of 100 mV s^{-1} and a prebias stabilization time of 2 s; calibration of the light intensity was done by a standard Si-based reference cell. The dark J-V curves of the devices were measured with the same procedure under dark conditions. The operational stability was determined with the same equipment and light source without any filter. A shadow mask with an active area of 0.04 cm^2 was used. The EQE and integrated current curves were measured by a home-built setup, with the photon flux calibrated by a set of optical power detectors (Newport: Models 818-SL and 818-IR). The impedance spectroscopy measurements were carried out at frequency from 0.1 to 10^6 *Hz* under dark/illumination and open circuit/short circuit condition.

SEM images of the perovskite surface were recorded with NovaNano SEM 650 with an acceleration voltage of 10 *kV*. AFM images were collected using a Bruker Multimode height microscope with ScanAsyst mode with a 512 points-per-line resolution. XRD patterns were measured on an X-ray powder diffractometer (D8 Advance, Bruker) with Cu Kα radiation and Lynxeye detector in air without any encapsulation. GIWAXS data were collected using a MINA X-ray scattering instrument equipped with a Cu rotating anode source (λ_{avg} = 1.5418 Å), with the incident angle set at 0.2° and 2° to investigate the surface and the bulk of the perovskite films, respectively. FTIR spectra were performed using a Shimadzu IRTracer100 in transmission mode. UV–vis absorbance spectra of the films were recorded with a Shimatzu UV—vis–NIR spectrophotometer (UV 3600) in transmission mode. Steady-state and time-resolved photoluminescence spectra (PL) measurements were obtained by exciting the samples with the second harmonic (400 nm) of a mode-locked Ti:sapphire laser (Mira 900, Coherent), and a pulse picker was used to reduce the laser repetition rate of 76 *MHz*. PL was collected in transmission geometry using a pair of achromatic doublets and a 435 nm long pass filter. Steady-state PL was measured using an Andor iDus 2.2 µm camera, and time-resolved PL using a Hamamatsu S1streak camera in single sweep mode.

Supporting Information

Supporting Information is available from the Wiley Online Library or from the author.

Acknowledgements

L.C. and F.T. contributed equally to this work. This publication is part of the Netherlands Organization of Scientific Research (NWO) – focus on "Next Generation Organic Photovoltaics", participating in the Dutch Institute for Fundamental Energy Research (DIFFER). This work was partially funded by the European Union's Horizon 2020 program, through a FET Proactive research and innovation action under grant agreement No. 101084124 (DIAMOND). F.T. thanks the Italian Ministry of Research for cofinancing a PhD position under the PON "Ricerca e Innovazione" 2014–2020 program FSE REACT-EU, decree 1061/2021. A.G. acknowledges partial funding from project PE0000021, "Network 4 Energy Sustainable Transition-NEST", Spoke 1, funded by European Union – Next Generation EU under NRRP, Mission 4, Component 2, Investment 1.3-Call for tender no. 1561 of the Italian Ministry of Research.

Conflict of Interest

The authors declare no conflict of interest.

Data Availability Statement

The data that support the findings of this study are available from the corresponding author upon reasonable request.

Keywords

lead-tin perovskites, low toxic solvent, nonradiative recombination, solar cells, two-step blade coating

Received: December 17, 2024
Revised: May 9, 2025
Published online:

[1] O. Almora, G. C. Bazan, C. I. Cabrera, L. A. Castriotta, S. Erten-Ela, K. Forberich, K. Fukuda, F. Guo, J. Hauch, A. W. Y. Ho-Baillie, T. J. Jacobsson, R. A. J. Janssen, T. Kirchartz, R. R. Lunt, X. Mathew, D. B. Mitzi, M. K. Nazeeruddin, J. Nelson, A. F. Nogueira, U. W. Paetzold, B. P. Rand, U. Rau, T. Someya, C. Sprau, L. Vaillant-Roca, C. J. Brabec, *Adv. Energy Mater.* **2024**, *15*, 189.

[2] H. Chen, C. Liu, J. Xu, A. Maxwell, W. Zhou, Y. Yang, Q. Zhou, A. S. R. Bati, H. Wan, Z. Wang, L. Zeng, J. Wang, P. Serles, Y. Liu, S. Teale, Y. Liu, M. I. Saidaminov, M. Li, N. Rolston, S. Hoogland, T. Filleter, M. G. Kanatzidis, B. Chen, Z. Ning, E. H. Sargent, *Science* **2024**, *384*, 189.
[3] J. Li, H. Liang, C. Xiao, X. Jia, R. Guo, J. Chen, X. Guo, R. Luo, X. Wang, M. Li, M. Rossier, A. Hauser, F. Linardi, E. Alvianto, S. Liu, J. Feng, Y. Hou, *Nat. Energy* **2024**, *9*, 308.
[4] B. Ehrler, E. Alarcón-Lladó, S. W. Tabernig, T. Veeken, E. C. Garnett, A. Polman, *ACS Energy Lett.* **2020**, *5*, 3029.
[5] L. Krückemeier, U. Rau, M. Stolterfoht, T. Kirchartz, *Adv. Energy Mater.* **2020**, *10*, 1902573.
[6] S. Albrecht, B. Rech, *Nat. Energy* **2017**, *2*, 16196.
[7] S. Shao, Y. Cui, H. Duim, X. Qiu, J. Dong, G. H. ten Brink, G. Portale, R. C. Chiechi, S. Zhang, J. Hou, M. A. Loi, *Adv. Mater.* **2018**, *30*, 1803703.
[8] M. Pitaro, J. E. S. Alonso, L. Di Mario, D. G. Romero, K. Tran, J. Kardula, T. Zaharia, M. B. Johansson, E. M. J. Johansson, R. C. Chiechi, M. A. Loi, *Adv. Funct. Mater.* **2024**, *34*, 2306571.
[9] Y. Zhang, C. Li, H. Zhao, Z. Yu, X. Tang, J. Zhang, Z. Chen, J. Zeng, P. Zhang, L. Han, H. Chen, *Nat. Commun.* **2024**, *15*, 6887.
[10] S. Hu, K. Otsuka, R. Murdey, T. Nakamura, M. A. Truong, T. Yamada, T. Handa, K. Matsuda, K. Nakano, A. Sato, K. Marumoto, K. Tajima, Y. Kanemitsu, A. Wakamiya, *Energy Environ. Sci.* **2022**, *15*, 2096.
[11] H. Chen, Z. Peng, K. Xu, Q. Wei, D. Yu, C. Han, H. Li, Z. Ning, *Sci China Mater.* **2021**, *64*, 537.
[12] R. Lin, Y. Wang, Q. Lu, B. Tang, J. Li, H. Gao, Y. Gao, H. Li, C. Ding, J. Wen, P. Wu, C. Liu, S. Zhao, K. Xiao, Z. Liu, C. Ma, Y. Deng, L. Li, F. Fan, H. Tan, *Nature* **2023**, *620*, 994.
[13] H. S. Kim, Y. J. An, J. Il Kwak, H. J. Kim, H. S. Jung, N. G. Park, *ACS Energy Lett.* **2022**, *7*, 1154.
[14] a) R. Vidal, J. A. Alberola-Borràs, S. N. Habisreutinger, J. L. Gimeno-Molina, D. T. Moore, T. H. Schloemer, I. Mora-Seró, J. J. Berry, J. M. Luther, *Nat. Sustain.* **2021**, *4*, 277; b) C. Fda, U.S. Food and Drug Administration. Q3C-Tables and List Guidance for Industry **2018**.
[15] Y. Cui, S. Wang, L. Ding, F. Hao, *Adv. Energy Sustainability Res.* **2021**, *2*, 2000047.
[16] D. Di Girolamo, J. Pascual, M. H. Aldamasy, Z. Iqbal, G. Li, E. Radicchi, M. Li, S. H. Turren-Cruz, G. Nasti, A. Dallmann, F. De Angelis, A. Abate, *ACS Energy Lett.* **2021**, *6*, 959.
[17] X. Meng, T. Wu, X. Liu, X. He, T. Noda, Y. Wang, H. Segawa, L. Han, *J. Phys. Chem. Lett.* **2020**, *11*, 2965.
[18] Y. Miao, M. Ren, Y. Chen, H. Wang, H. Chen, X. Liu, T. Wang, Y. Zhao, *Nat. Sustain.* **2023**, *6*, 1465.
[19] S. Lv, W. Gao, G. Xing, L. Chao, L. Song, M. Li, L. Fu, Y. Chen, C. Ran, *ACS Appl. Mater. Interfaces* **2022**, *14*, 43362.
[20] Z. Tang, S. Wang, W. Zhu, L. Ding, F. Hao, *Green Chem.* **2023**, *25*, 1150.
[21] A. Yadegarifard, H. Lee, H. J. Seok, I. Kim, B. K. Ju, H. K. Kim, D. K. Lee, *Nano Energy* **2023**, *112*, 108481.
[22] R. M. I. Bandara, S. M. Silva, C. C. L. Underwood, K. D. G. I. Jayawardena, R. A. Sporea, S. R. P. Silva, *Energy Environ. Mater.* **2022**, *5*, 370.
[23] J. Yang, E. L. Lim, L. Tan, Z. Wei, *Adv. Energy Mater.* **2022**, *12*, 2200975.
[24] J. X. Zhong, W. Q. Wu, L. Ding, D. B Kuang, *Energy Environ. Mater.* **2021**, *4*, 277.
[25] Y. C. Kim, H. J. An, D. H. Kim, J. M. Myoung, Y. J. Heo, J. H. Cho, *Adv. Funct. Mater.* **2021**, *31*, 2005553.
[26] X. Jiang, J. Zhang, X. Liu, Z. Wang, X. Guo, C. Li, *Angew. Chem., Int. Ed.* **2022**, *61*, 202115663.
[27] H. B. Lee, N. Kumar, B. Tyagi, S. He, R. Sahani, J. W. Kang, *Mater. Today Energy* **2021**, *21*, 100759.
[28] Y. Zhao, J. Wei, H. Li, Y. Yan, W. Zhou, D. Yu, Q. Zhao, *Nat. Commun.* **2016**, *7*, 10228.
[29] A. H. Proppe, A. Johnston, S. Teale, A. Mahata, R. Quintero-Bermudez, E. H. Jung, L. Grater, T. Cui, T. Filleter, C. Y. Kim, S. O. Kelley, F. De Angelis, E. H. Sargent, *Nat. Commun.* **2021**, *12*, 3472.
[30] X. Li, J. M. Hoffman, M. G. Kanatzidis, *Chem. Rev.* **2021**, *121*, 2230.
[31] X. Sheng, Y. Li, M. Xia, E. Shi, *J. Mater. Chem. A.* **2022**, *10*, 19169.
[32] L. Chen, E. K. Tekelenburg, K. Gahlot, M. Pitaro, J. Xi, A. Lasorsa, G. Feraco, L. Protesescu, P. C. A. van der Wel, G. Portale, P. Rudolf, C. J. Brabec, M. A. Loi, *Energy Environ. Sci.* **2023**, *16*, 5315.
[33] Y. Han, H. Xie, E. L. Lim, D. Bi, *Sol. RRL* **2022**, *6*, 2101007.
[34] D. Prat, A. Wells, J. Hayler, H. Sneddon, C. R. McElroy, S. Abou-Shehada, P. J. Dunn, *Green Chem.* **2016**, *18*, 288.
[35] P. A. Wender, T. E. Smith, H. A. Duong, J. Louie, E. A. Standley, S. Z. Tasker, *Encyclopedia of Reagents for Organic Synthesis*, Wiley, Hoboken, New Jersey **2015**.
[36] M. Anyfantakis, D. Baigl, *ChemPhysChem* **2015**, *16*, 2726.
[37] J. M. Wang, G. H. Liu, Y. L. Fang, W. K. Li, *Rev. Chem. Eng.* **2016**, *32*, 551.
[38] S. Sánchez, L. Pfeifer, N. Vlachopoulos, A. Hagfeldt, *Chem. Soc. Rev.* **2021**, *50*, 7108.
[39] Z. Wu, E. Bi, C. Li, L. Chen, Z. Song, Y. Yan, *Sol. RRL* **2023**, *7*, 2200571.
[40] X. Liu, T. Wu, X. Luo, H. Wang, M. Furue, T. Bessho, Y. Zhang, J. Nakazaki, H. Segawa, L. Han, *ACS Energy Lett.* **2022**, *7*, 425.
[41] D. P. Belotskii, I. N. Antipov, V. F. Nadtochii, S. M. Dodik, *Inorg. Mater.* **1969**, *5*, 1583.
[42] S. Lv, W. Gao, C. Ran, D. Li, L. Chao, X. Wang, L. Song, Z. Lin, L. Fu, Y. Chen, *Sol. RRL* **2021**, *5*, 2100675.
[43] W. Shen, H. Fang, D. Pu, W. Zheng, X. Zhang, G. Li, L. Huang, S. Zhou, W. Chen, Y. Zhou, Z. Feng, J. Liang, J. Zhou, P. Qin, G. Fang, W. Ke, *Adv. Funct. Mater.* **2024**, 2410605.
[44] S. Chen, X. Dai, S. Xu, H. Jiao, L. Zhao, J. Huang, *Science* **2021**, *373*, 902.
[45] J. K. Pious, H. Lai, J. Hu, D. Luo, E. Gilshtein, S. Siegrist, R. K. Kothandaraman, Z. H. Lu, C. M. Wolff, A. N. Tiwari, F. Fu, *ACS Appl. Mater. Interfaces* **2024**, *16*, 39399.
[46] Z. Yang, A. Rajagopal, C. C. Chueh, S. B. Jo, B. Liu, T. Zhao, A. K. Y. Jen, *Adv. Mater.* **2016**, *28*, 8990.
[47] W. Liao, D. Zhao, Y. Yu, N. Shrestha, K. Ghimire, C. R. Grice, C. Wang, Y. Xiao, A. J. Cimaroli, R. J. Ellingson, N. J. Podraza, K. Zhu, R. G. Xiong, Y. Yan, *J. Am. Chem. Soc.* **2016**, *138*, 12360.
[48] W. Chen, X. Li, Y. Li, Y. Li, *Energy Environ. Sci.* **2020**, *13*, 1971.
[49] D. Ingerle, G. Pepponi, F. Meirer, P. Wobrauschek, C. Streli, *Spectrochim. Acta Part B At Spectrosc.* **2016**, *118*, 20.
[50] X. Sun, D. Li, L. Zhao, Y. Zhang, Q. Hu, T. P. Russell, F. Liu, J. Wei, H. Li, *Adv. Mater.* **2023**, *35*, 2301115.
[51] R. Yang, R. Li, Y. Cao, Y. Wei, Y. Miao, W. L. Tan, X. Jiao, H. Chen, L. Zhang, Q. Chen, H. Zhang, W. Zou, Y. Wang, M. Yang, C. Yi, N. Wang, F. Gao, C. R. McNeill, T. Qin, J. Wang, W. Huang, *Adv. Mater.* **2018**, *30*, 1804771.
[52] D. Liang, C. Dong, L. Cai, Z. Su, J. Zang, C. Wang, X. Wang, Y. Zou, Y. Li, L. Chen, L. Zhang, Z. Hong, A. El-Shaer, Z. K. Wang, X. Gao, B. Sun, *Small* **2021**, *17*, 2102558.
[53] a) M. Liu, D. Zheng, T. Zhu, K. Vegso, P. Siffalovic, T. J. A. M. I. Pauporté, *Adv. Mater. Interfaces* **2024**, *11*, 2300773; b) H. Hu, S. Moghadamzadeh, R. Azmi, Y. Li, M. Kaiser, J. C. Fischer, Q. Jin, J. Maibach, I. M. Hossain, U. W. Paetzold, B. A Nejand, *Adv. Funct. Mater.* **2021**, *32*, 2107650.
[54] M. T. Khan, P. Huang, A. Almohammedi, S. Kazim, S. Ahmad, *iScience* **2021**, *24*, 102024.
[55] K. P. Goetz, F. T. F. Thome, Q. An, Y. J. Hofstetter, T. Schramm, A. Yangui, A. Kiligaridis, M. Loeffler, A. D. Taylor, I. G. Scheblykin, Y. Vaynzof, *J. Mater. Chem. C* **2023**, *11*, 8007.